

Influence of Connate Water and Condensate Saturation on Inertial Effects in Gas/Condensate Reservoirs

J.-M. Lombard, D.G. Longeron, SPE, and F.J.M. Kalaydjian, SPE, Inst. Français du Pétrole

Summary

In the near-wellbore region of gas/condensate wells, high-pressure gradients induce both large condensate saturation and high gas velocities which may lead to significant deviations from Darcy's law for gas permeability. At the present time, no physically relevant model exists which takes into account these non-Darcian two-phase flow phenomena. Using a specific laboratory equipment, a laboratory study has been performed with the aim to estimate the influence of pore structure and connate water saturation S_{wi} on the gas inertial coefficient β_g , and to integrate the effect of the condensate dropout in the Forchheimer flow equation. Experiments were conducted on sandpacks and sandstone core samples. For dry gas floods, the measured β_g values were found in good agreement with previous published data. For gas floods in presence of S_{wi} , β_g was found to increase with S_{wi} and a new correlation between β_g and a mean-pore radius \bar{r} is proposed. Gas/condensate (C_1 - C_3 mixtures) steady-state experiments showed that β_g values increased with the total liquid saturation.

Introduction

During the exploitation of gas/condensate reservoirs, the bottom-hole flowing pressure decreases gradually. Below the dewpoint pressure, retrograde condensation occurs leading to the segregation and then to the mobilization of the condensate phase (above the critical condensate saturation S_{cc}) towards the producing wells. The liquid phase accumulates in the wellbore region, forming a ring which progressively impairs the gas deliverability. In addition to that, steadily, the produced gas becomes lighter and, therefore, less marketable. Predicting reservoir gas performance and economy thus requires an accurate modeling of the flow behavior and the thermodynamics of those processes.

In the reservoir, far from the wellbore, flow rates are low and Darcy's law remains valid. It is possible to reproduce in the laboratory such flow rates and to study the fluid behavior. Some authors¹⁻⁵ studied the evolution of the critical condensate saturation with the gas-liquid interfacial tension (IFT). They measured gas and condensate relative permeabilities and correlated them with a capillary number.

But near the wellbore, high-pressure gradients induce both large condensate saturation and high gas velocities which may lead to significant deviations from Darcy's law for the gas permeability. The near-wellbore region plays a key role in the productivity decline of the field, and at the present time, no physically relevant model exists which takes into account these non-Darcian two-phase flow effects. A better description of flowing properties may lead to a better prediction of the productivity decline.

Background. Much research has been conducted to understand the failure of Darcy's law when the gas flow rate is gradually increased.⁶⁻¹⁰ In 1914, Forchheimer⁶ proposed the following equation, which is still the most commonly used flow equation:

$$-\partial p/\partial x = \mu/kv + \beta\rho v^2, \quad (1)$$

where μ/k is the viscous Darcy's term and β is called the inertial coefficient. Noman and Archer⁴ and Kalaydjian *et al.*³ summarized the origin of inertial effects and the influence of fluids and pore structure on β . In the case of an immobile liquid saturation, many correlations like Geertsma's¹¹ exist, which express β as a function of porosity, permeability, and gas saturation, namely,

$$\beta \sim 1/(k^{0.5}\phi^{5.5}S_g^{5.5}). \quad (2)$$

Inertial effects for a gas phase flowing at high flow rates in a porous medium appear to be stronger in the presence of a mobile liquid rather than a nonmobile one.¹² But, this has never been supported by any conclusive experiment and no reliable correlations still exist. For gas/condensate flow, Coles and Hartman¹³ developed a method to estimate the effective β_g coefficient at different liquid saturations: they used core samples containing various saturations of solidified paraffin wax that mimic an immobile condensate phase. But, these experiments were performed under ambient conditions. In addition, at high liquid saturation, above the critical, immobile paraffin is not representative of a mobile liquid. Consequently, to take into account inertial effects, the Forchheimer equation is generally implemented in reservoir simulators with a $\beta_g(k, \phi, S_{wi})$ correlation established for an immobile liquid saturation. However, neither the mobility of the liquid nor thermodynamic conditions are considered. In the case of a gas/condensate field, this leads to a large inaccuracy in the prediction of well productivity.

For gas/condensate fields, pioneering numerical simulation works were performed by Gondouin *et al.*¹⁴ However, inertial effects under reservoir conditions have never been experimentally studied. Acquiring such laboratory data is important to establish and validate any correlation.

This paper presents an improvement of the description of gas/condensate flowing properties in the near-wellbore region. A specialized laboratory equipment has been built at the Institut Français du Pétrole (IFP) in order to perform high-velocity gas/condensate displacements, as representative as possible of near-wellbore conditions. With this equipment, a methodology was developed to measure the effective β_g coefficient for gas and gas/condensate displacements. Single-phase flow experiments were conducted to evaluate the influence of pore structure and S_{wi} on β_g value. Gas/condensate displacements were performed to quantify the effect of condensate saturation on the Forchheimer flow equation. Experiments performed with consolidated and unconsolidated porous media, and with analog gas/condensate systems, are reported and the results are discussed.

Equipment and Procedures

Apparatus. It is quite difficult to model in the laboratory pressure and temperature wellbore flow conditions. Typically, a field production flow rate q_{field} (7 MPa; 37.8°C) of 10⁶ m³/day leads in the laboratory to 111 L/h³ (core diameter=4 cm), using a C_1 - C_3 binary fluid as an analog of a real gas/condensate system.

In order to reach such high flow rates under pressure and temperature and to simulate the wellbore flow conditions, the prototype Pegase has been developed at IFP (Ref. 15) (**Fig. 1**). Its main specifications are: the capability to inject a large volume of fluid in the porous medium at fixed pressure drop ($\Delta p_{max}=20$ bar), by means of two high flow rate pumps, and a good pressure regulator and an accurate control of flow rates.

Copyright © 2000 Society of Petroleum Engineers

This paper (SPE 65430) was revised for publication from paper SPE 56485, presented at the 1999 SPE Annual Technical Conference and Exhibition held in Houston, 3-6 October. Original manuscript received for review 11 November 1999. Revised manuscript received 1 June 2000. Manuscript peer approved 5 June 2000.

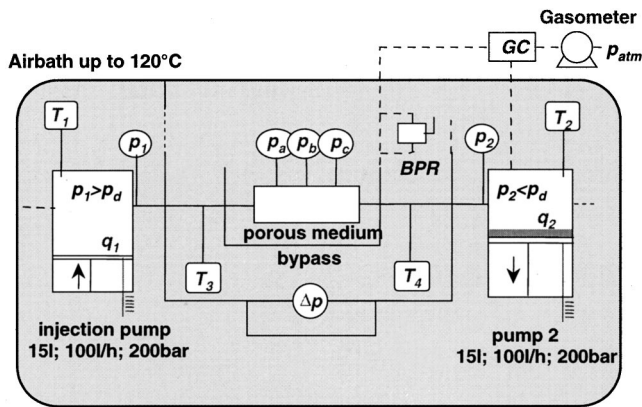


Fig. 1—Pegase prototype.

Measurement of β_g : Gas Flow Case. The objective is to study the influence of pore structure (k, ϕ, S_{wi}) on inertial effects during gas displacement. To measure the β_g coefficient of various porous media, the following steps were taken.

- Initially, the system (pumps and porous medium) is saturated with gas at a given pressure p_1 ($p_1 = 90$ bar, for instance).

- The outlet pressure is reduced step by step down to selected values $p_2(i) = p_1 - \Delta p(i)$, while pump 1 continuously injects gas in the porous medium, at the constant pressure p_1 . At each pressure step (i), the inlet and outlet flow rates adjust themselves. Once equilibrium is reached, that is, once the flow parameters are stable, flow rates $q_1(i)$ and $q_2(i)$, pressures p_1 and $p_2(i)$, and differential pressure $\Delta p(i)$ are recorded and the outlet pressure is automatically reduced down to the next step value $p_2(i+1)$.

- The curves $\partial p_1 / \partial x$ vs. q_1 and $\partial p_2 / \partial x$ vs. q_2 can be drawn with the equilibrium values and the deviation of Darcy's law should be observed.

- β_g is deduced while plotting the pressure-squared difference over the mass flow rate vs. the mass flow rate q_m ($q_m = \rho q$). The slope of the curve gives β_g , and the extrapolation of the ratio for $q_m = 0$ gives the effective permeability k_g (Fig. 2).

Remark. The integration of the Forchheimer equation

$$(p_1^2 - p_2^2) / (2\mu L c q_m / s) = 1/k_g + \beta_g / \mu q_m / s, \quad (3)$$

with $c = zRT/M$ (M is the universal gas constant), supposes that the variations of z (compressibility) and μ (viscosity) between p_1 and p_2 are small enough to be considered negligible. For nitrogen (N_2), between 90 and 70 bar, the viscosity μ and the compressibility factor z do not vary drastically and the integration in Eq. 3 can be applied (Table 1).

Measurement of β_g : Gas/Condensate Case. The objective is to study the influence of the condensate saturation of the β_g coefficient, that is, to draw the Forchheimer curves $(p_1^2 - p_2^2) / p_1 q_1$ vs. q_m , at various condensate saturations S_c (Fig. 3). A well-known C_1 - C_3 mixture is considered at constant temperature. The following steps are taken.

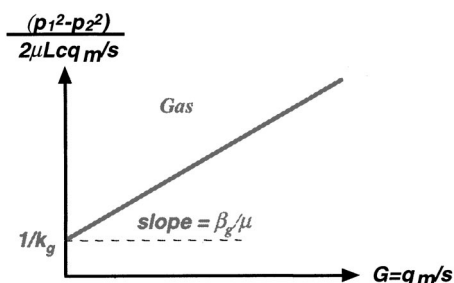


Fig. 2—Evaluation of β_g coefficient.

TABLE 1—NITROGEN PROPERTIES AT 21°C

p (bar)	μ (cp)	z	ρ (kg/m ³)
1	0.0176	0.9998	1.15
5	0.0176	0.9989	5.74
10	0.0177	0.9979	11.49
70	0.0189	0.9953	80.66
80	0.0191	0.9966	92.06
90	0.0194	0.9985	103.37

- Initially, the porous medium is saturated with gas in the presence of connate water saturation. The pore pressure is above the dewpoint pressure p_d ($p_1 = p_2 > p_d$).

- Pressure step (i): the fluid is injected in the porous medium at a constant pressure p_1 slightly above p_d , while the outlet pressure is regulated at a constant selected value $p_2(i)$ below the dewpoint. In the porous medium, near the inlet, the pressure becomes lower than p_d and a condensate appears. This liquid accumulates and above the critical saturation S_{cc} , it becomes mobile. Once pressures and flow rates are stabilized, they are measured.

Fig. 4 shows the shape of pressure and condensate saturation profiles obtained through simulations at this “dynamic” equilibrium. If p_1 is not far from p_d ($p_1 - p_d < 1$ bar), one-dimensional (1D) simulations show that local $[S_c(i, x)]$ and average $[S_c(i)]$ condensate saturations are very narrow (1 to 2%).

- $S_c(i)$ measurement: when the dynamic equilibrium is reached, the porous medium is isolated. The pore pressure stabilizes to the average pressure $\bar{p}_p(i)$ and a new saturation profile is obtained (Fig. 5). The average condensate saturation corresponding to this “static” equilibrium, $S_c[\bar{p}_p(i)]$, is deduced from a material balance made during a miscible injection of C_1 , with gas chromatography (GC) analysis of the effluent. 1D simulations show that this saturation and the average saturation $S_c(i)$ of the dynamic equilibrium are comparable (2 to 5%).

Steps 2 and 3 are repeated for different values of $p_2(i)$. Finally, the coefficient β_g is correlated with the average condensate saturation $S_c[\bar{p}_p(i)]$.

β_g is a function of S_c . For its measurement (Fig. 3), S_c should be fixed. In a four-step experiment with a given C_1 - C_3 mixture, each step (i) corresponds to a pressure $p_2(i)$ and to a condensate saturation $S_c(i)$. For each step (i) there is only one point in the Forchheimer diagram relative to $S_c(i)$ (Fig. 6). For a given S_c , a minimum of three C_1 - C_3 mixtures are needed to obtain three points in the Forchheimer diagram (Fig. 7). To reach a given S_c , the pressure conditions for each mixture have to be estimated. These conditions can be chosen by means of iterative simulations: after the experiment with a first fluid (first point in the Forchheimer diagram), the displacement of the second C_1 - C_3 mixture is simulated with the IFP numerical simulator ATHOS™ and an average saturation is calculated. The pressure conditions are then modified in order to obtain the same S_c as for the first fluid. The experiment performed at these calculated pressures gives a second point in the Forchheimer diagram. The same operation is per-

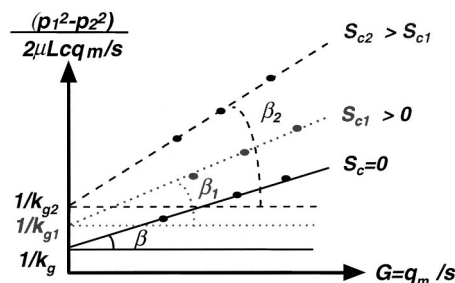


Fig. 3—Measurement of $\beta_g(S_c)$, principle.

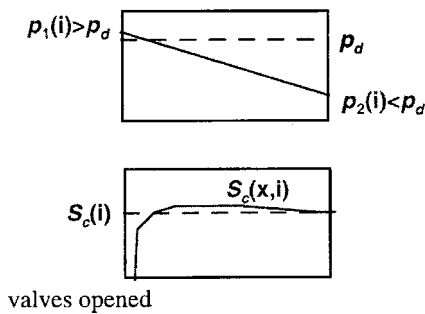


Fig. 4— p and S_c profiles in dynamic equilibrium.

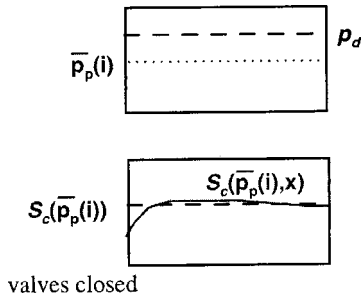


Fig. 5— p and S_c profiles in static equilibrium.

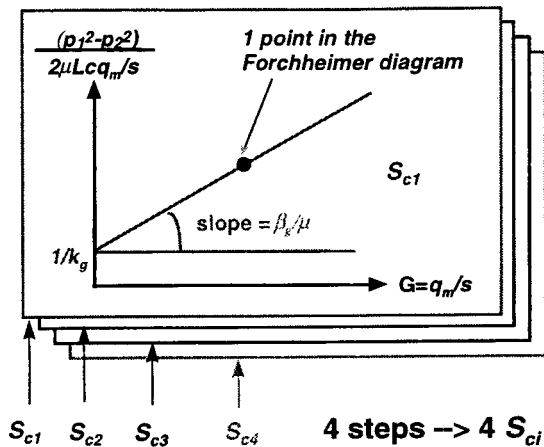


Fig. 6—Four-step experiment with one C_1 - C_3 mixture.

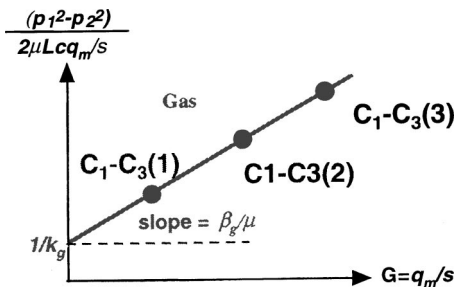


Fig. 7—Experiments with three C_1 - C_3 mixtures at fixed S_c .

TABLE 2—POROUS MEDIA

Porous Medium	L (cm)	d (cm)	ϕ (%)	PV (cm^3)	k_w (md)	k_{N_2} (md)	\bar{d}^* (μm)
V4-2B	40	4.87	21.9	163.9	169	211	8
B1B	24.85	4.85	15.8	72.5	28	40	3.5
ST1	613.5	0.6	37.9	65.7	2430	2510	~49
ST2	1000	0.6	36.3	102.6	2710	2670	~50

* \bar{d} is the average pore diameter corresponding to 50% of nonwetting saturation (from the mercury pore size-distribution curve).

formed for the third fluid to obtain a third point in the Forchheimer diagram (Fig. 7). An example of such simulations is given in the next section.

Porous Media and Fluids. Two sandstone core samples were selected from a computerized tomography (CT) scan examination: a Vosges sandstone (V4-2B: medium permeability) and a Birchover sandstone (B1B: low permeability). Gas (nitrogen) and brine (30 g/L KCl) permeabilities were measured. Some experiments were performed at connate water saturation S_{wi} . To establish S_{wi} brine was first displaced by viscous oil. This was followed by successive floods of light oil, methane, and, finally, nitrogen. The brine saturation profiles were checked for uniformity (CT-scan analysis before and after displacements). No significant heterogeneity of the profiles was detected. Experiments were also performed on two slim tubes, ST1 and ST2, filled with calibrated glass beads (diameter: 20 to 40 μm). Table 2 shows the dimensions and the main characteristics of these porous media.

The experiments in single-phase conditions were performed with nitrogen and air (for slim tubes) at ambient temperature (cf. N_2 properties in Table 1).

For a gas/condensate experiment, it has been shown that, instead of real fluids, analog fluid systems can be used to measure gas/condensate flow parameters.³ The main advantage of using analog fluid systems like C_1 - C_3 mixtures is that, contrary to actual fluids, the pressure and temperature to be applied are not too high. At 38°C, the dewpoint pressure is about 90 bar whatever the composition of the C_1 - C_3 mixture may be. Table 3 gives the composition and the maximum liquid dropout (MLDO) at 38°C of the three C_1 - C_3 mixtures selected for the study. Fig. 8 shows that the interfacial tension of C_1 - C_3 mixtures do not vary drastically with pressure between 80 and 90 bar at 38°C (0.02 to 0.09 mN/m). The constant volume depletion (CVD) curves were determined experimentally at 38°C (Fig. 9) and were compared with the ones calculated with the IFP pressure/volume/temperature (PVT) simulator. As shown in Table 3, PVT simulations overestimate the maximum liquid dropout (MLDO). This effect is due to the fact that at 38°C we are near the critical point (Fig. 10). In this region, it is well known that PVT calculations are never very accurate and overestimate the liquid dropout. Furthermore, experimentally, near the critical point a small impurity can drastically modify the thermodynamic equilibrium.

Results and Discussion

Single-Phase Flow Experiments. The inertial gas coefficient was determined for the Vosges and Birchover sandstones and for the two slim tubes at various connate water saturations, following the above-described procedure. The results are grouped in Table 4. Fig. 11 shows the deviation from Darcy's law observed for the dry Vosges sandstone. The Forchheimer diagram used to estimate the β_g coefficient is presented in Fig. 12. The measurements are reproducible (cf. measurements on V4-2B at $S_{wi}=0.34$, Table 4). In Table 4, measured β_g values are compared with the ones calculated from the Geertsma correlation (expressed in SI units):

$$\beta_g = 0.005 / (\phi^{5.5} k_w^{0.5}) \quad \text{for } S_{wi}=0 \quad (k_w \text{ in } \text{m}^2; \beta_g \text{ in } \text{m}^{-1}), \quad (4)$$

Fluid	C ₁ (mol %)	C ₃ (mol %)	MLDO exp. (liq %)	MLDO calc. (liq %)	p _d exp. (bara)	p _d calc. (bara)
1	59	41	8.2	17.6	89.1	90.7
2	56	44	~20	47.9	91	91.4
3	54.5	45.5	31.4	70.6	91	90.5

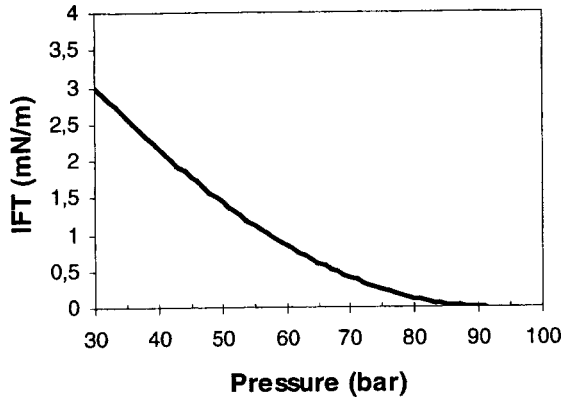


Fig. 8—IFT of C₁-C₃ mixtures at 38°C.

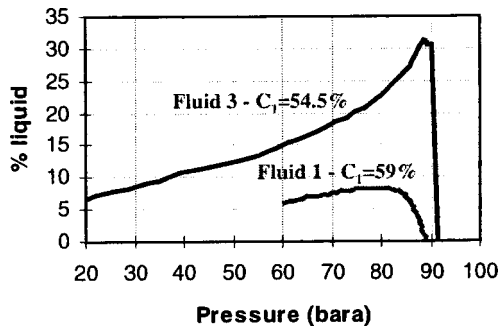


Fig. 9—Experimental CVD of Fluids 1 and 3 at 38°C.

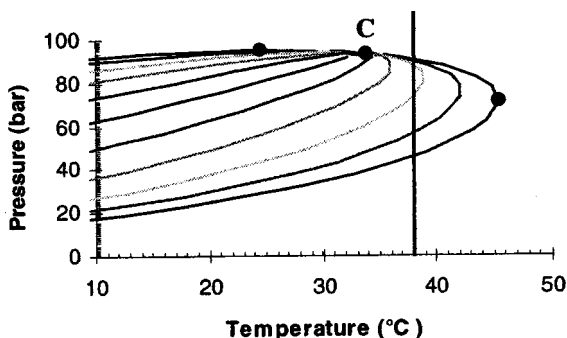


Fig. 10—Simulated phase envelope of fluid 1 (C₁=59 mol %).

$$\beta_g = 0.005[\phi^{5.5}(1 - S_{wi})^{5.5}k_g^{0.5}]$$

for $S_{wi} > 0$ (k_g in m²; β_g in m⁻¹). (5)

The experimental values are quite different from the calculated ones. As has also been observed in the literature, the Geertsma correlation overestimates inertial effects, particularly if water is present in the porous medium.

Fig. 13 shows an increase of β_g with the water saturation for both sandstones, consistent with what is reported in the literature. The presence of water reduces the available pore volume and, consequently, saturation and permeability. It increases the number of direction changes and the flow path length of the fluid and, consequently, the pressure losses and the β_g value. In Fig. 14 measured values are compared to literature data.¹⁶ They are in good agreement with previous published results. Fig. 14 shows a decrease in inertial effects with increase in permeability, as generally observed.

An attempt was made to reconcile the values obtained with and without S_{wi} . For each porous medium and each water saturation, an average equivalent pore radius \bar{r} was calculated using the following formula (Table 5):

$$\bar{r} = (8.k_w / \phi)^{0.5} \quad (\text{USI}) \quad \text{for } S_{wi} = 0, \quad (6)$$

$$\bar{r} = [8.k_g / \phi(1 - S_{wi})]^{0.5} \quad (\text{USI}) \quad \text{for } S_{wi} > 0. \quad (7)$$

These formulas, established for bundles of identical capillaries from Poiseuille and Darcy's equations, lead to a good linear relationship: $\log \beta_g$ vs. \bar{r} for all experiments (Fig. 15). The inertial coefficient decreases as the equivalent pore radius increases, which is when the permeability increases or when the water saturation decreases.

Gas/Condensate High Flow Rate Displacements. Gas/condensate displacements were performed in the Birchover sandstone (B1B at $S_{wi} = 24.8\%$ PV, Table 2) with the C₁-C₃ mixtures given in Table 3 and following the above-described procedure.

Simulation Example. As explained in the previous session, 1D simulations were performed in order to estimate the operating conditions. For these simulations, the k_r values used were measured with nitrogen and decane at $S_{wi} = 24.8\%$ PV. At 38°C and between 90 and 70 bar, the interfacial tension of C₁-C₃ mixtures is small and does not vary drastically (Fig. 8). An average value of IFT=0.05 mN/m was used to deduce the gas-liquid capillary pressure curve from the mercury injection curve.

The injections of three selected C₁-C₃ mixtures in the B1B sample were simulated using 100 homogeneous cells. The injection pressure p_1 was constant: $p_1 = 90/91$ bar ($p_1 > p_d$). The outlet pressure was reduced step by step down to 72 bar. For each outlet pressure p_2 at dynamic equilibrium, the flow rates, the pressure profile, and the saturation profile were calculated. The average pressure and saturation of the porous medium were then deduced from these profiles. With such simulations, it is possible to approximately estimate for each fluid the experimental conditions, that is, pressures p_1 and p_2 , leading to an average condensate saturation. But, simulations do not take into account the influence of S_c on β_g . Consequently, these pressure values are only approximations, and experimentally they have to be adjusted to obtain a proper average S_c .

TABLE 4—MEASURED AND CALCULATED INERTIAL COEFFICIENTS

Porous Medium	S_{wi} (%PV)	Measured					Geertsma Correlation			
		β_g (m ⁻¹)	β_g (ft ⁻¹)	ϕ	k_w (darcy)	k_g (darcy)	$\beta_g(S_{wi}=0)$ (m ⁻¹)	$\beta_g(S_{wi}>0)$ (m ⁻¹)	$\beta_g(S_{wi}=0)$ (ft ⁻¹)	$\beta_g(S_{wi}>0)$ (ft ⁻¹)
V4-2B	0	1.30E+08	3.96E+07	0.219	0.169	0.211	5.16E+07		1.57E+07	
V4-2B	34	1.92E+08	5.85E+07	0.219	...	0.208		4.57E+08		1.39E+08
V4-2B	34	1.90E+08	5.79E+07	0.219	...	0.208		4.57E+08		1.39E+08
V4-2B	40	2.80E+08	8.53E+07	0.219	...	0.096		1.14E+09		3.46E+08
B1B	0	1.12E+09	3.41E+08	0.158	0.028	0.04	7.63E+08		2.33E+08	
B1B	24.8	2.20E+09	6.71E+08	0.158	...	0.033		3.37E+09		1.03E+09
B1B	43	5.60E+09	1.71E+09	0.158	...	0.025		1.78E+10		5.42E+09
ST1 air	0	4.08E+05	1.24E+05	0.379	2.43	2.53	6.66E+05		2.03E+05	
ST1 N ₂	0	4.49E+05	1.37E+05	0.379	2.43	2.51	6.66E+05		2.03E+05	
ST1	18.3	5.74E+05	1.75E+05	0.379	...	2.02		2.22E+06		6.77E+05
ST2 air	0	4.11E+05	1.25E+05	0.363	2.71	2.69	8.00E+05		2.44E+05	
ST2 N ₂	0	4.02E+05	1.23E+05	0.363	2.71	2.67	8.00E+05		2.44E+05	

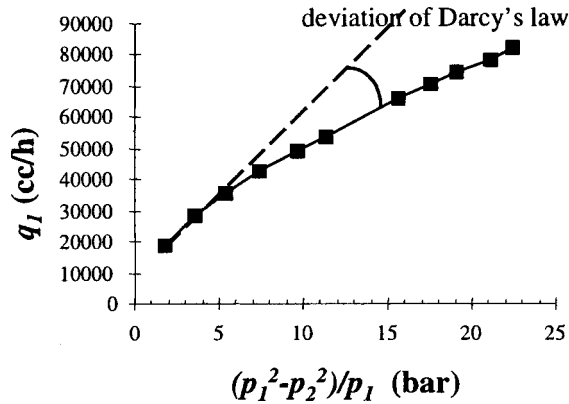


Fig. 11—V4-2B at $S_{wi}=0$: deviation of Darcy's law.

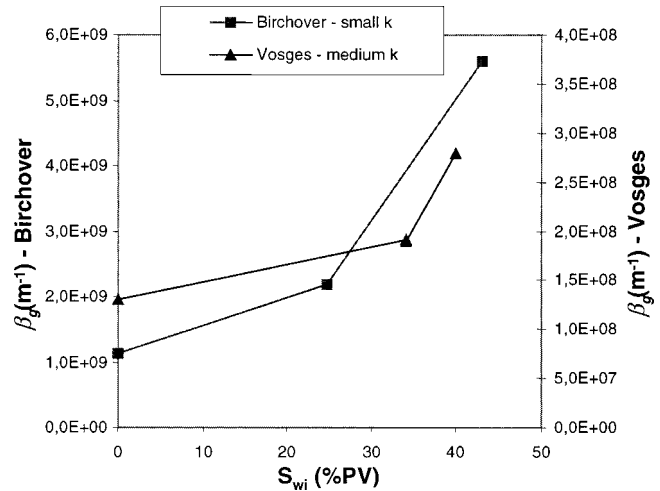


Fig. 13—Evolution of β_g with S_{wi} .

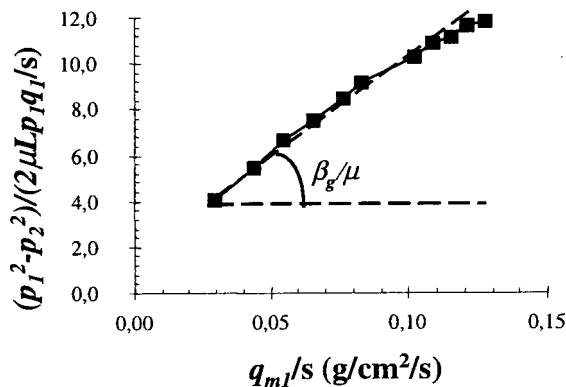


Fig. 12—V4-2B at $S_{wi}=0$: β_g measurement.

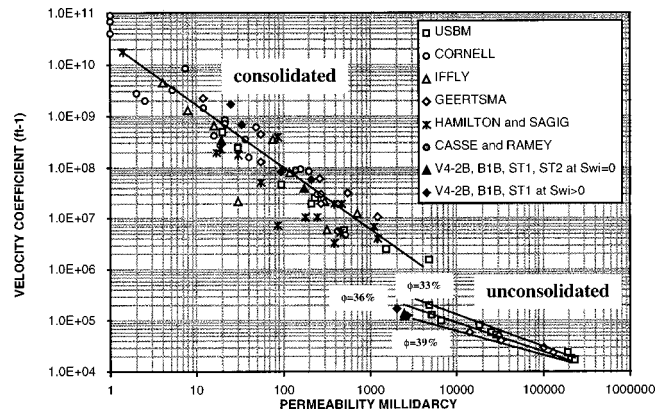


Fig. 14—Correlation of β_g with permeability (see Ref. 16).

Porous medium	ϕ	S_{wi} (% PV)	k_w (md)	k_g (md)	β_g (m^{-1})	\bar{r} (μm)
V4-2B	0.219	0	169	211	1.3E+08	2.48
V4-2B	0.219	34	...	208	1.9E+08	3.39
V4-2B	0.219	40	...	96	2.8E+08	2.42
B1B	0.158	0	28	40	1.1E+09	1.19
B1B	0.158	24.8	...	33	2.2E+09	1.49
B1B	0.158	43	...	25	5.6E+09	1.49
ST1	0.379	0	2430	2510	4.5E+05	7.16
ST1	0.379	18.3	...	2020	5.7E+05	7.23
ST2	0.363	0	2710	2670	4.0E+05	7.73

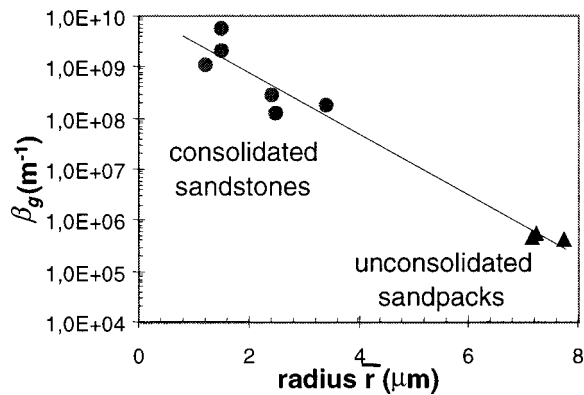


Fig. 15—Correlation β_g vs. r .

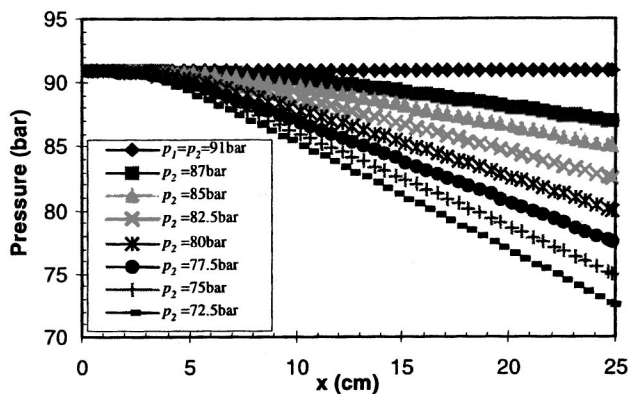


Fig. 16—Simulation of C_1 - C_3 injection in the B1B sample at 38°C; pressure profiles at equilibrium.

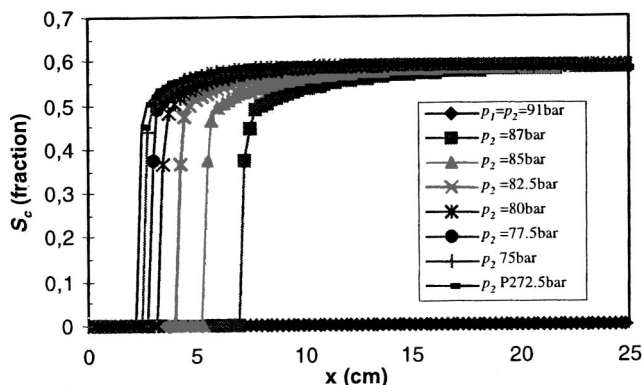


Fig. 17—Simulation of C_1 - C_3 injection in the B1B sample at 38°C; condensate saturation profiles at equilibrium.

Figs. 16 and 17 show examples of pressure and condensate saturation profiles obtained at each equilibrium step for the injection of fluid 1 ($C_1=59\%$) in the B1B sample. No influence of the capillary pressure on the results was found.

Experimental Results. For each fluid and each pressure step (i), the best regulation parameters (proportional bands of pumps) were selected in order to reach equilibrium. The results of all experiments performed are presented in Fig. 18. On this Forchheimer diagram error bars relative to the equilibrium flow rate measurements are reported for each point. Squares denote measurements with the first fluid ($C_1=59\%$) and circles with the third fluid ($C_1=54.5\%$). The measured condensate saturation is indicated for each point.

As expected, all the points relative to a nonzero condensate saturation are located above the reference line $S_c=0$ ($\beta_g = 2.2 \times 10^9 m^{-1}$). The presence of condensate increases inertial effects.

In Fig. 18, it is difficult to interpret all the results in term of a β_g variation with S_c (as in Fig. 3). At a given S_c value, it is not possible to find a linear correlation as for the gaseous case ($S_c = 0$). For some experiments, the pressure and flow rate stabilization was poor, implying large error bars ($C_1=59\%$, $S_c=0.47, 0.57,$ and 0.75). The stabilization of the flow rate was really better for the rich fluid ($C_1=54.5\%$, circles in Fig. 18). With this fluid, the maximum condensate dropout is high, liquid appeared more rapidly in the porous medium, leading to high stable condensate saturation. Furthermore, the uncertainty in the calculation of the average saturation is difficult to estimate. In addition to experimental inaccuracy due to different thermodynamic conditions, the measured saturation $S_c[\bar{p}_p(i)]$ (Fig. 5: porous medium isolated, $p = \bar{p}_p(i)$, no pressure gradient) may be slightly different from the saturation $S_c(i)$ (Fig. 4: dynamic equilibrium $p_1 > p_d > p_2$) at which pressures and flow rates were measured.

Interpretation. For some experiments, the measured values of the condensate saturation were quite narrow ($S_c=55, 58, 60.2,$ and 61.0% PV). Considering that these experiments have been performed at the same condensate saturation (average value S_c

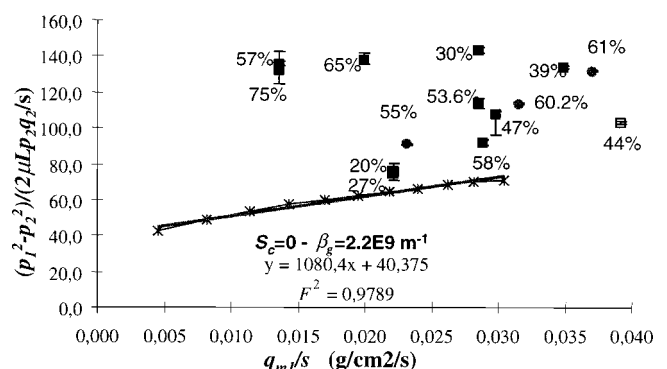


Fig. 18—Gas/condensate displacements in B1B at $S_{wi} = 24.8\%$ PV, Forchheimer diagram.

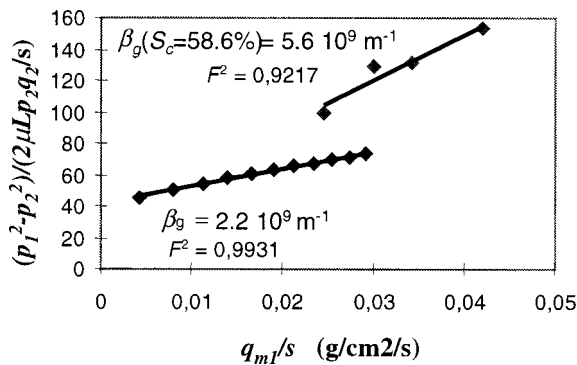


Fig. 19— β_g value of B1B at $S_{wi}=24.8\%$ PV and $S_c=58.6\%$ PV.

=58.6% PV), it is possible to estimate a β_g value. Fig. 19 presents the Forchheimer diagram relative to $S_c=58.6\%$ PV. The slope of the curve leads to the coefficient $\beta_g(S_c=58.6\% \text{ PV})=5.6 \cdot 10^9 \text{ m}^{-1}$ with a good correlation factor ($F^2=0.92$). This value is much higher than the one obtained at $S_c=0$, since it is increased by a factor 2.5.

Conclusions

A specific laboratory equipment and methodology were developed and used to determine the inertial gas coefficient β_g for single-phase flow and for gas/condensate displacements. The following conclusions were drawn: for single-phase flow, β_g is higher for consolidated porous media than for unconsolidated porous media. β_g increases as the permeability decreases and as water saturation increases [for the Birchover sandstone, that is, for the less-permeable sample, $\beta_g(S_{wi}=0.43)=5 \cdot \beta_g(S_w=0)$]. β_g is well correlated and decreases with the average pore radius \bar{r} .

For gas/condensate experiments, the presence of condensate increases the inertial effects. For an average condensate saturation of 58.6%, β_g was found to be significantly higher than the value measured at zero-condensate saturation (factor 2.5). These results obtained with C_1 - C_3 mixtures must be confirmed with other analog gas/condensate systems like C_1 - C_4 mixtures, far from critical conditions, to improve the measurement of the condensate saturation. One concludes that neglecting the effect of water and condensate saturation on β_g may lead to an overestimation of well productivity indices.

Future Work. To establish $\beta_g(S_c)$ correlations other experiments must be performed at different condensate saturation values with other fluids. To reduce the uncertainty on the equilibrium flow rates it would be better to work with rich fluids. Furthermore, Fig. 10 showed that at 38°C, a C_1 - C_3 mixture is near the critical point. This temperature is only 3.5°C higher than the critical temperature of fluid 3. In this region, the thermodynamic properties are difficult to calculate, and experimentally, the equilibrium is very sen-

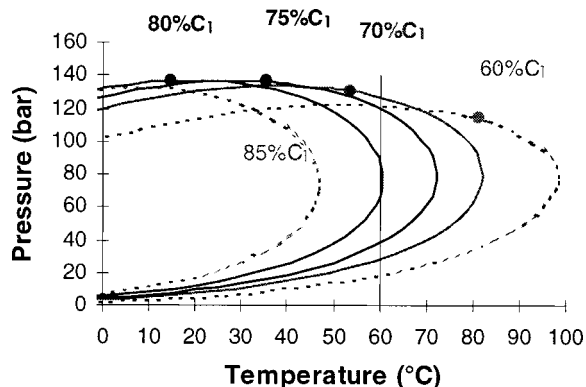


Fig. 20—Phase envelope of C_1 - C_4 mixtures.

sitive to any impurity. To avoid these problems and to work far from the critical point, C_1 - C_4 mixtures could be used: actually, calculations show that a working temperature of 60°C is, respectively, 6.5 and 45.5°C higher than the critical temperature of C_1 - C_4 mixtures with a composition of $C_1=70\%$ and $C_1=80\%$ (Fig. 20). The calculated CVD curves of these C_1 - C_4 mixtures at 60°C give liquid dropouts in the range 2 to 25%.

Nomenclature

d	= core diameter, L, m
\bar{d}	= average pore diameter, L, m
F	= correlation factor
k_g	= effective gas permeability, L^2, m^2
k_r	= relative permeability
k_w	= absolute water permeability, L^2, m^2
L	= core length, L, m
M	= molar weight, g/mol
p	= pressure, m/Lt ² , bar
P_c	= capillary pressure, m/Lt ² , bar
p_c	= critical pressure, m/Lt ² , bar
p_d	= dewpoint pressure, m/Lt ² , bar
\bar{p}_p	= average pore pressure, m/Lt ² , bar
q	= flow rate, L ³ /t, m ³ /s
q_m	= mass flow rate, m/t, kg/s
\bar{r}	= average equivalent pore radius, L, m
s	= core section, L ² , m ²
S_c	= condensate saturation
S_{cc}	= critical condensate saturation
S_g	= gas saturation
S_l	= liquid saturation
S_{or}	= residual oil saturation
S_{wi}	= connate water saturation
T	= temperature, °C
T_c	= critical temperature, °C
v	= velocity, L/t, m/s
z	= compressibility factor
β	= inertial coefficient, L ⁻¹ , m ⁻¹
Δp	= differential pressure, m/Lt ² , bar
ϕ	= porosity, fraction
ρ	= density, m/L ³ , g/cm ³
μ	= viscosity, m/Lt, cp

Subscripts

1	= inlet
2	= outlet
c	= critical
g	= gas (vapor) phase
(i)	= pressure step
i	= irreducible
w	= water

Acknowledgments

This research program has been partly funded by an industrial consortium involving AGIP, Gaz de France, Sonatrach, and Total. We wish to acknowledge the members of this consortium for their permission to publish these results, and for their valuable discussions and insights which contributed to the completion of the work.

References

- Henderson, G.D. *et al.*: "An Investigation Into the Processes Governing Flow and Recovery in Different Flow Regimes Present in Gas/Condensate Reservoirs," paper SPE 26661 presented at the 1993 SPE Annual Technical Conference and Exhibition, Houston, 3–6 October.
- Henderson, G.D. *et al.*: "Measurement and Correlation of Gas/Condensate Relative Permeability by the Steady-State Method," paper SPE 30770 presented at the 1995 SPE Annual Technical Conference and Exhibition, Dallas, 22–25 October.
- Kalaydjian, F.J.-M., Bourbiaux, B.J., and Lombard, J.-M.: "Predicting Gas/Condensate Reservoir Performance: How Flow Parameters are Altered When Approaching Production Wells," paper SPE 36715 presented at the 1996 SPE Annual Technical Conference and Exhibition, Denver, Colorado, 6–9 October.

4. Noman, R. and Archer, J.S.: "The Effect of Pore Structure on Non-Darcy Gas Flow in Some Low-Permeability Reservoir Rocks," paper SPE 16400 presented at the 1987 SPE/DOE Low-Permeability Reservoirs Symposium, Denver, Colorado, 18–19 May.
5. Gravier, J.F. *et al.*: "Determination of Gas/Condensate Relative Permeability on Whole Cores Under Reservoir Conditions," *SPEFE* (February 1986) 9; *Trans.*, AIME, **281**.
6. Forchheimer, P.: "Wasserbewegung durch Boden," *Zeit. Ver. Deutsch. Ing.* (December 1901) **45**, 1781.
7. Fancher, G.H. and Lewis, J.A.: "Flow of Simple Fluids Through Porous Materials," *Ind. Eng. Chem.* (October 1933) **25**, 1139.
8. Cornell, D. and Katz, D.L.: "Flow of Gases Through Consolidated Porous Media," *Ind. Eng. Chem.* (October 1953) 2145.
9. Tek, M.R.: "Development of a Generalized Darcy Equation," *Trans.*, AIME (1957) **210**, 376.
10. Tek, M.R., Coats, K.H., and Katz, D.L.: "The Effect of Turbulence on Flow of Natural Gas Through Porous Reservoirs," *JPT* (July 1962) 799; *Trans.*, AIME, **225**.
11. Geertsma, J.: "Estimating the Coefficient of Inertial Resistance in Fluid Flow Through Porous Media," *SPEJ* (October 1974) 445.
12. Wong, S.W.: "Effect of Liquid Saturation on Turbulence Factors for Gas Liquid Systems," *J. Cdn. Pet. Tech.* (October–December 1970) 274.
13. Coles, M.E. and Hartman, K.J.: "Non-Darcy Measurements in Dry Core and Effect of Immobile Liquid," paper SPE 39977 presented at the 1998 SPE Gas Technology Symposium, Calgary, 15–18 March.
14. Gondouin, M., Iffly, R., and Husson, J.: "An Attempt To Predict the Time Dependence of Well Deliverability in Gas/Condensate Fields," *SPEJ* (June 1967) 113; *Trans.*, AIME, **240**.
15. Lombard, J.-M., Longeron, D., and Kalaydjian, F.: "Well Productivity of Gas/Condensate Fields: Influence of Connate Water and Condensate Saturation on Inertial Effects," paper SCA 9929 presented at 1999 Intl. Symposium of the Soc. of Core Analysts, Golden, Colorado, 1–4 August.
16. Firoozabadi, A. and Katz, D.L.: "An Analysis of High-Velocity Gas Flow Through Porous Media," *JPT* (February 1979) 211.

SI Metric Conversion Factors

bar × 1.0*	E+05 = Pa
cp × 1.0*	E−03 = Pa·s
dyn/cm × 1.0*	E+00 = mN/m
ft × 3.048*	E−01 = m
ft ³ × 2.831 685	E−02 = m ³
lbm × 4.535 924	E−01 = kg

*Conversion factors are exact.

SPEJ

Jean-Marc Lombard is with the Inst. Français du Pétrole (IFP) in Rueil Malmaison, France, where he is in charge of studies on productivity of decline of gas/condensate fields and on water-imbibition processes in fractured porous media. e-mail: j-marc.lombard@ifp.fr. With IFP since 1992, he has worked with the Reservoir Engineering Dept. on the influence of wettability on fluid flows in porous media, gravity drainage, high flow rates, gas/condensate, and waterflood. Lombard holds a PhD degree in petroleum sciences from IFP and Pierre & Marie Curie U. **Daniel Longeron** is a principal research engineer with IFP in Rueil Malmaison and Manager of the Well Injectivity and Productivity Team, where he supervises theoretical and experimental studies related to near-wellbore flow properties. e-mail: daniel.longeron@ifp.fr. Longeron holds a degree in physics and chemistry from the U. of Paris and degree in drilling, production, and reservoir engineering from Ecole Natl. Supérieure des Mines de Paris (ENSPM)/IFP. He is chairman of the Europec 2000 Program Committee and served on a 1992–95 Annual Meeting Technical Committee. **François Kalaydjian** is Director of the Reservoir Engineering Research Div. at IFP in Rueil Malmaison. e-mail: francois.kalaydjian@ifp.fr. He has previously spent 5 years as a project leader for IFP. He has been involved for more than 10 years in studies related to modeling of fluid-flow phenomena in porous media, including three-phase flow, gas injection, gas/condensate, and water imbibition in fractured media. Kalaydjian holds an engineering degree from ENSPM and a PhD degree in physics from the U. of Bordeaux.